ACS OMEGA

http://pubs.acs.org/journal/acsodf

Article

Enrichment of Residual Carbon in Coal Gasification Fine Slag via Wet Sieving Separation with Ultrasonic Pretreatment

Meijie Sun, Suqian Gu, Dinghua Liu,* Zhiqiang Xu, Weidong Wang, Yanan Tu, Lufan Wang, Haiyan Liu, and Sijia Lu

Cite This: *ACS Omega* 2022, 7, 40306−40315

Read Online

ACCESS | Metrics & More | Article Recommendations

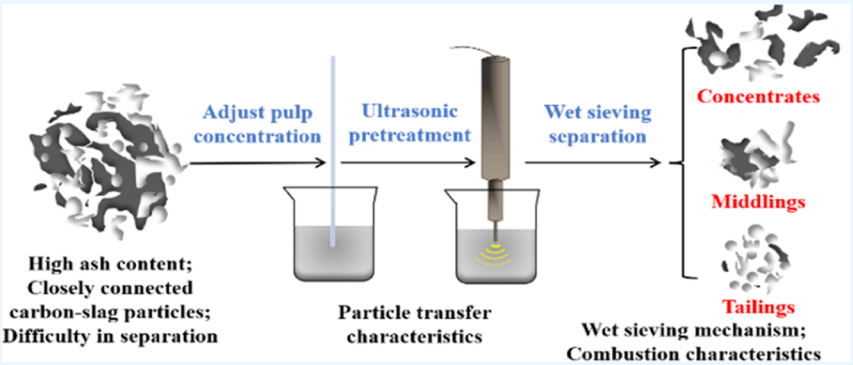

ABSTRACT: To overcome the environmental and economic challenges posed by the increasing amounts of the coal gasification slag, here, a simple and efficient method for enriching the residual carbon from the coal gasification fine slag was proposed. The residual carbon enrichment pattern in the particle size distribution of coal gasification fine slags after the ultrasonic pretreatment was mainly enriched toward the 500−250 μm and 250−125 μm particle size classes by analyzing the changes in the particle size distribution and apparent morphology. The pulp pretreatment at the ultrasonic output power of 270 W for 4 min was determined as the optimal experimental condition with respect to the yield, ash content, and ash rejection of the concentrates. Compared to the conventional wet sieving separation, the yield and ash content of the final concentrates were reduced by 7.99 and 14.96%, respectively. Moreover, the ash rejection of the final concentrates was as high as 88.51%, indicating an increment of 11.63% than the conventional wet sieving separation. Furthermore, thermogravimetric analysis confirmed that the final concentrates exhibited the lowest reactivity; however, these demonstrated had the highest carbon content (nearly 70%) with 27.27% ash content. The combustion characteristics analysis showed that the wet screening concentrate after ultrasonic pretreatment had the highest composite combustion characteristic index (S) of 3.17×10^{-8}, as compared to the raw and conventional sieving concentrates.

1. INTRODUCTION

The coal gasification process is critical to the diversification and low-carbon energy development of the world's energy sources, especially for developing countries.[1,2] For instance, coal consumption for coal gasification process in China exceeds 200 million tons per year, while several million tons of coal gasification slag are generated.[3] However, the gasification slag, which contains harmful substances such as tar, sulfur-containing catalysts, and various salts, is a typical hazardous waste. For the sake of environmental safety and economic considerations, a large extent of the coal gasification slag needs to be recycled.

Due to the advantages of high carbon conversion, wide range of raw materials, and environmental protection, the entrained-flow coal gasification process has been developed significantly in recent years compared with other coal gasification processes. The gasification process of the pulverized coal in the entrained-flow gasifier is described in Figure 1,[4,5] whereas the schematic diagram of the slag treatment system is shown in Figure 2.[6] Compared with coarse slag, fine slag is richer in residual carbon with a higher economic value. However, previous studies have shown that the reaction properties of high carbon fines are poor[7,8] and unsuitable for secondary gasification or combustion. In addition, the landfill or stacking of coal gasification slag not only causes waste of resources but also pollutes the

Received: August 14, 2022
Accepted: October 18, 2022
Published: October 25, 2022

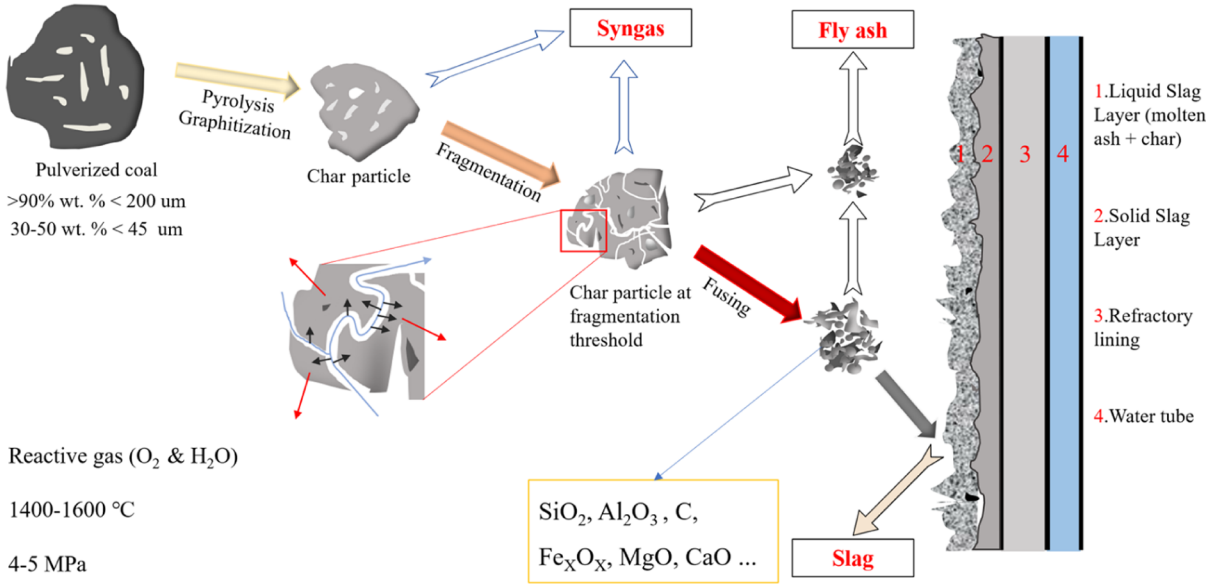

Figure 1. Gasification process of the pulverized coal in an entrained-flow gasifier.

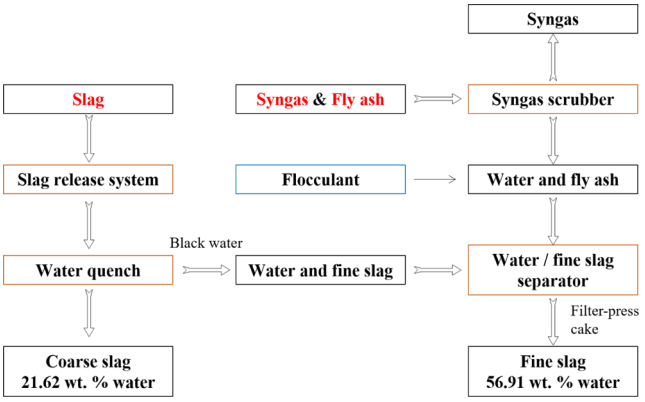

Figure 2. Flow chart of the slag treatment system in an entrained-flow gasifier.

surrounding environment.[9] Therefore, it is necessary to enrich and recover the residual carbon in the coal gasification slag, especially for the fine slag, to improve the economic and environmental benefits for coal gasification enterprises.

In the last decade, the mineral processing methods, including flotation and sieving, have been widely used to separate and enrich the residual carbon from the coal gasification fine slag. In entrained flow coal gasification furnaces, the closely embedded molten ash and residual carbon are stripped off by reactive gases at high temperatures and then quenched in a water bath, which leads to significant oxidation and large surface area of the particles.[10−12] Therefore, it is difficult to obtain additional economic value from the enrichment of carbon residues by flotation due to the excessive flotation reagents required. In addition, the research studies have shown that the fine slag has obvious grading characteristics as it contains a variety of products collected in the entrained-flow coal gasifier. Thus, the different size fractions in the residual carbon differ in content and characteristics,[13−15] indicating that the residual carbon can be effectively enriched through simple sieving.

However, the enrichment of the residual carbon in the fine slag by sieving separation suffers from a significant challenge. The molten ash and residual carbon are often closely embedded, in particular, a large number of the high ash fine particles are attached on the surface of the partly gasified carbon particles.[16] Such a unique tightly wrapped combination makes it nearly impossible to achieve an effective separation even by mechanical stirring and wet sieving, thus, leading to a high ash content in the concentrates as well a low separation efficiency. Indeed, for closely embedded minerals, the effective dissociation, cleaning and dispersion are often prerequisites for an efficient separation.[17] However, for the fine slag, the natural particle size is remarkably fine and the mixing degree is high; thus, the grinding dissociation further increases with mixing, leading to a reduced separation accuracy. The rupture of cavitation bubbles can generate high-speed shock waves and micro-spray during the ultrasonic pretreatment of pulp.[18,19] The mechanical effects generated by this process can clean the surface of particles,[20,21] broken particles,[22] emulsified reagents, and so forth. Therefore, ultrasonic processing is a relatively gentle separation method, which can largely disperse the high ash fines adhering on the surface of fine slag particles and thus improving the separation efficiency of wet sieving.

Our previous study[18] reported that the ultrasonic pretreatment can improve the residual carbon recovery efficiency from the coal gasification fine slag, and reduce the ash content and change the particle size distribution of the flotation concentrates at the same time. Different ultrasonic pretreatment conditions were employed to pretreat the pulp with a certain concentration modulated by the fine slag and water. These systematic studies and concrete conclusions are envisaged to lead to numerous practical applications. The obtained findings have a certain guiding influence on the separation and purification of the mixed solid waste exhibiting grading characteristics, such as waste lithium batteries[23] and fly ash.[24,25] Moreover, the separation experiments employed in the study were simple and efficient, thus representing swift extension to the relevant research and industrial production.

In this work, the effect of ultrasonic pretreatment on the enrichment of residual carbon from the coal gasification fine slag through wet sieving separation was investigated comprehensively. First, the variation in the particle size

https://doi.org/10.1021/acsomega.2c05220
ACS Omega 2022, 7, 40306−40315

Table 1. Proximate Analysis and High Heating Value of XFS, Conventional Wet Sieving Separation, and Wet Sieving Separation with Ultrasonic Pretreatment[a]

sample	M_{ad}/%	A_{ad}/%	V_{ad}/%	FC_{ad}/%	V_{daf}/%	HHV/MJ·kg^{-1}
XFS	2.42	61.86	3.94	31.78	11.03	10.30
XFS-0(0)-M	1.98	43.30	4.10	50.62	7.50	17.55
XFS-0(0)-C	2.41	41.21	3.93	52.45	6.98	18.15
XFS-0(0)-T	2.03	79.53	3.31	15.13	17.95	3.78
XFS-270(4)-M	1.83	56.19	4.55	37.43	10.83	12.71
XFS-270(4)-C	2.67	26.54	2.24	68.56	3.16	23.64
XFS-270(4)-T	2.27	76.89	3.64	17.19	17.48	4.66

[a]M_{ad}, A_{ad}, V_{ad}, and FC_{ad} refer to moisture, ash, volatile, and fixed carbon on an air-dry basis, whereas V_{daf} refers to volatile on a dry ash-free basis.

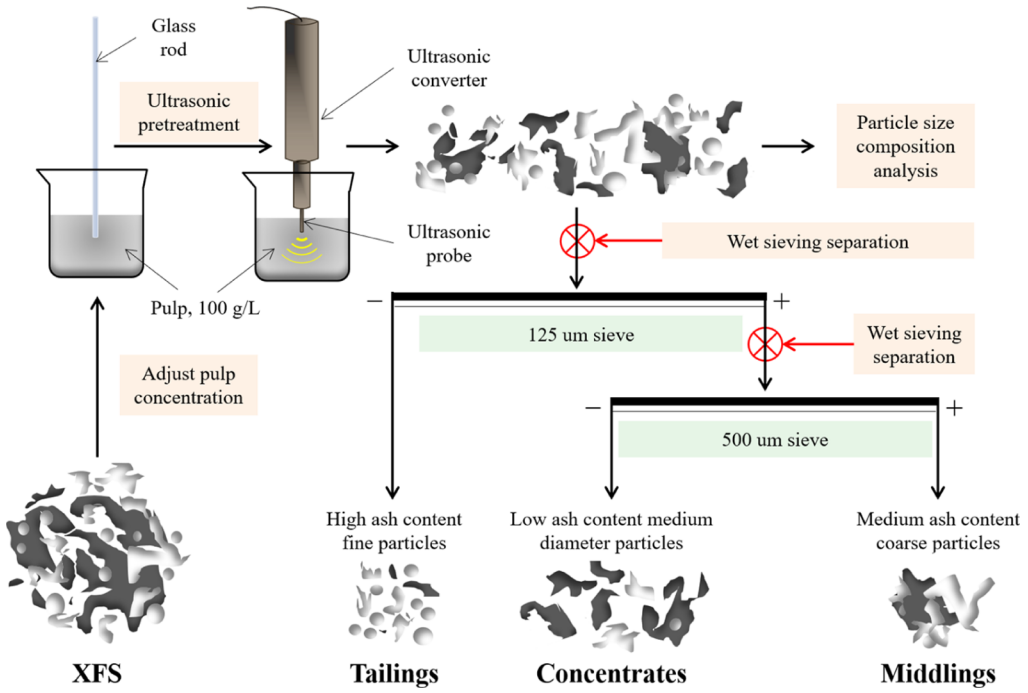

Figure 3. Wet sieving separation experiment process and the research flow.

distribution of the samples as a function of the ultrasonic pretreatment conditions was studied, followed by the establishment of the transfer rule of the residual carbon after ultrasonic pretreatment. Second, by employing an industrial CCD camera, each particle size fraction during the conventional and ultrasonic pretreatment wet sieving was imaged, and the apparent morphological changes in each particle size fraction were compared. Third, the optimal separation conditions were determined by quantifying the yield, quality, and ash rejection (AR) of the calculated concentrates. Final, the non-isothermal thermogravimetric analysis (TG-DTG) was used to characterize the combustion performance of the original sample, conventional wet sieving products and ultrasonically pretreated wet sieving products. This work aims to provide some theoretical foundation on the realization of the goal of "harmlessness, recycling, and utilization" for the coal gasification slags via a combination of ultrasonic pretreatment and wet sieving process.

2. MATERIALS AND METHODS

2.1. Materials. The coal gasification fine slag, named as XFS, was procured from a typical entrained-flow coal gasification plant in Xinjiang, China. Because the moisture content of the initial XFS was 56.91%, the experimental samples were dried at 105 °C for 6 h and subsequently air dried for 12 h. The proximate analysis[26,27] and high heating value of XFS was presented in Table 1. The fixed carbon content of XFS was as high as 31.78%, indicating its potential recovery value for the coal gasification plants. Besides, the volatile content of 3.94% indicated the lower reactivity, and therefore, it was not suitable for direct gasification. The high heating value was calculated according to the relation: HHV = −0.03 A_{ad} − 0.11 M_{ad}+0.33 V_{ad} + 0.35 FC_{ad}.[28] XFS-0(0)-C, XFS-0(0)-M, and XFS-0(0)-T referred to the concentrates, middlings, and tailings obtained after the conventional wet sieving separation, respectively. On the other hand, XFS-270(4)-C, XFS-270 (4)-M and XFS-270(4)-T represented the concentrates, middlings, and tailings obtained after the wet sieving separation with 270 W ultrasonic pretreatment for 4 min.

2.2. Ultrasonic Pretreatment Process. Mixing 60 g of XFS and 600 mL of water in a beaker stirred at low speed for 2 min. A TL-1800Y ultrasonic equipment was applied in the ultrasonic pretreatment for the coal gasification slag. The ultrasonic output power range was 0−1800 W and the frequency was 20 kHz, and the magnitude of the ultrasonic output energy was represented by the percentage of the maximum ultrasonic output power. In this study, 0, 90, 180,

https://doi.org/10.1021/acsomega.2c05220
ACS Omega 2022, 7, 40306−40315

270, and 360 W ultrasonic output powers were selected for the pulp pretreatment over a period of 4 min and the samples signed as XFS-0(0), XFS-90(4), XFS-180(4), XFS-270(4), and XFS-360(4), respectively. Furthermore, the samples pretreated by ultrasonic time of 0, 2, 4, 6, and 8 min at 270 W were defined as XFS-0(0), XFS-270(2), XFS-270(4), XFS-270(6), and XFS-270(8), respectively.

2.2.1. Particle Size Distribution Analysis. The particle size distribution analyses of the samples were conducted based on the Chinese National Standard GB/T 477-2008. The tests were carried out using a set of sieves, including 500, 250, 125, 75, and 45 μm. Each particle size fraction was sequentially filtered, dried, and weighed, and then, the ash content was measured. The tests were repeated three times, with the average value of the test results reported as the final value.

2.2.2. Apparent Morphology of the Particle Fractions. Using a GP-660V industrial CCD camera, each particle size fraction for the conventional and ultrasonic pretreatment (270 W for 4 min) wet sieving was imaged, and the changes in apparent morphologies for each fraction were compared. The corresponding scales have been marked in the images.

2.3. Calculation of Concentrate Parameters. The separated products were divided into three types after different ultrasonic pretreatment conditions. The fraction below 125 μm contained the fine particles with high ash content, named as tailings. The product in the range 125−500 μm included the medium diameter particles with low ash content, termed as concentrates. The fraction with >500 μm particles consisted of the coarse particles with medium ash content, denoted as middlings. The yield of concentrates $\gamma_C(\%)$ and AR are calculated by using Eqs 1 and 2[29,30]

$$\gamma_C(\%) = \frac{m_C}{m_F} \times 100\% \tag{1}$$

$$\begin{aligned} \mathrm{AR}(\%) &= 100 - \text{Ash recovery}(\%)\ \textit{in}\ \text{concentrates} \\ &= 100 - \frac{\gamma_C \bullet A_C}{A_F} \end{aligned} \tag{2}$$

where, m_C, m_F, A_C, andA_F represent the concentrates mass (g), the feed weight (g), the ash content of the concentrates (%), and the feed ash content (%), respectively.

The wet sieving separation experiment process and the research flow are shown in Figure 3.

2.4. Thermogravimetric Analysis. *2.4.1. TGA Equipment and Test Method.* To verify the combustibility of XFS and ultrasonically pretreated wet sieving products, their combustion characteristics were investigated by TG-DTG curves. The XFS was sieve separated by using two sieves of size 125 and 500 μm in the conventional and ultrasonic pretreatment wet sieving processes for obtaining the representative samples. Three products for each method were subsequently obtained.

HCT-2 TGA unit was used for the TGA. About 10 mg of dry samples were weighed for the combustion experiment. The TGA experiments were conducted in an air environment from 25.5 to 900 °C with the heating rate of 7 °C/min and an airflow rate of 50 mL/min. The mass loss (%) curves were plotted as a function of the temperature, and the derivative thermogravimetric (%/°C) curves were obtained by differentiating the TG curves, followed by the generation of the DTG (%/min) curves for the final analysis by multiplying the derivative curves with the heating rate.[31] Each sample was tested at least twice to confirm the reproducibility.

2.4.2. Determination of Combustion Characteristic Parameters. The combustion characteristic parameters could be determined from the TG-DTG curves,[32,33] including ignition temperature (T_i), maximum weight loss rate temperature (T_{peak}), corresponding maximum weight loss rate (dW_{max}), burnout temperature (T_h), average weight loss rate (dW_{mean}), and so forth. Figure 4 gives the TG-DTG curves and

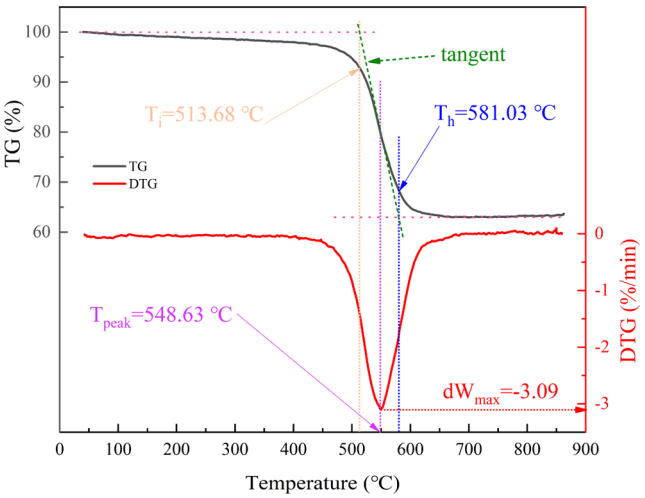

Figure 4. TG-DTG curves and related characteristic parameters of XFS.

the related characteristic parameters for the XFS sample. A vertical line was drawn along the lowest point of the DTG curve, intersecting with the TG curve. Then, a tangent line was drawn at the intersection that intersected the horizontal line of the initial combustion phase. The temperatures corresponding to the two points were considered as T_{peak} and T_i, respectively. Based on these parameters, the flammability index (C) and composite combustion characteristic index (S) of the sample can be calculated by using Eqs 3 and 4[34]

$$C = \frac{dW_{max}}{T_i^2} \tag{3}$$

$$S = \frac{dW_{max} \bullet dW_{mean}}{T_i^2 \bullet T_h} \tag{4}$$

The higher the C value, the better the ignition stability of the sample. Besides, the S value reflected comprehensively the ignition and burnout performance of the sample. Moreover, the larger the S value, the superior the comprehensive combustion performance of the sample.[35]

3. RESULTS AND DISCUSSION

3.1. Variation in the Particle Size Distribution of the Samples. *3.1.1. Undersize Cumulative Yield.* Figure 5a shows the undersize cumulative yield for each ultrasonic output power and Figure 5b demonstrates the undersize cumulative yield as a function of the ultrasonic pretreatment time. On enhancing the output power and pretreatment time, the undersize cumulative yield curve was noted to move to the left as a whole, and the d_{80} value decreased accordingly. The cleaning, crushing, and dispersion action associated with the ultrasonic treatment effectively reduced the particle size and

https://doi.org/10.1021/acsomega.2c05220
ACS Omega 2022, 7, 40306−40315

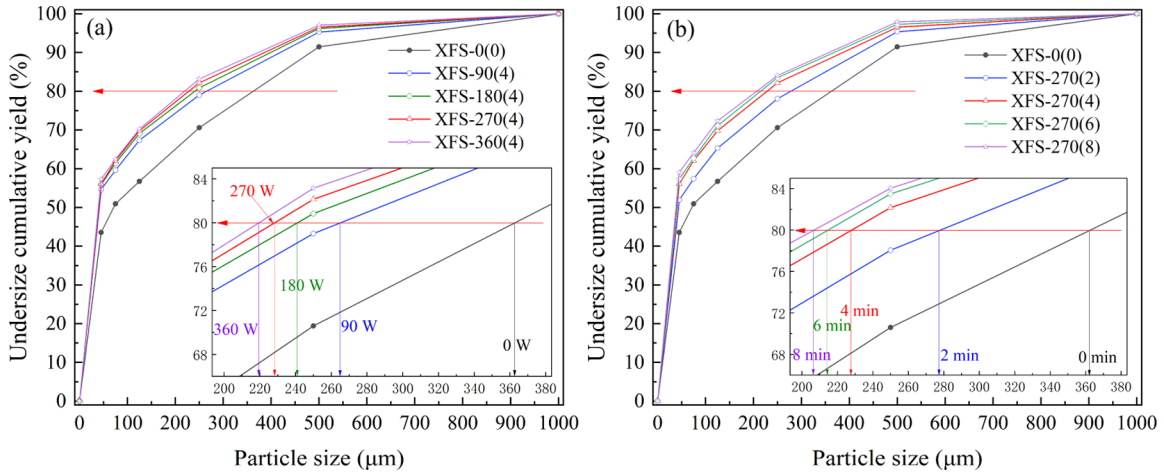

Figure 5. Undersize cumulative yield as a function of the ultrasonic output power (a) and ultrasonic pretreatment time (b).

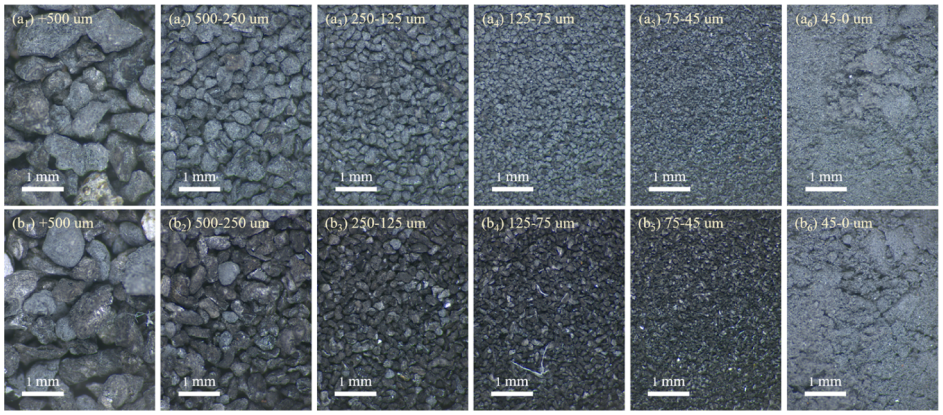

Figure 6. Apparent morphologies of the different particle size fractions in conventional wet sieving (a_1−a_6) and wet sieving with ultrasonic pretreatment (b_1−b_6).

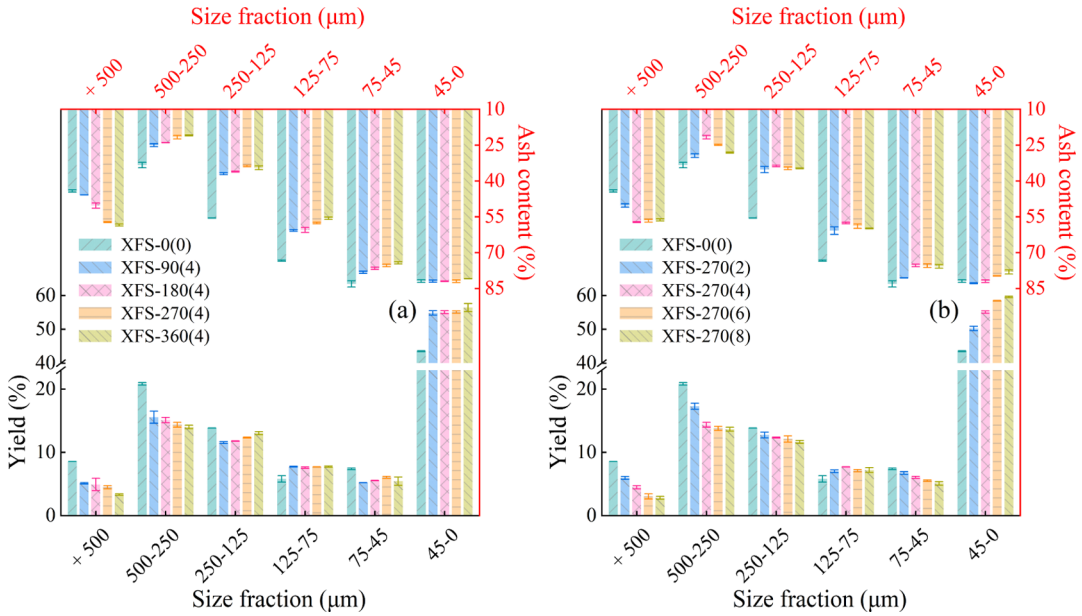

Figure 7. Yield and ash content of the different particle size fractions as a function of the ultrasonic output power (a) and ultrasonic pretreatment time (b).

thus reducing the content of the coarse particles and enhancing the content of the fine particles.[36] Therefore, the ultrasonic pretreatment exerted a significant effect on the particle size distribution of XFS.

https://doi.org/10.1021/acsomega.2c05220
ACS Omega 2022, 7, 40306−40315

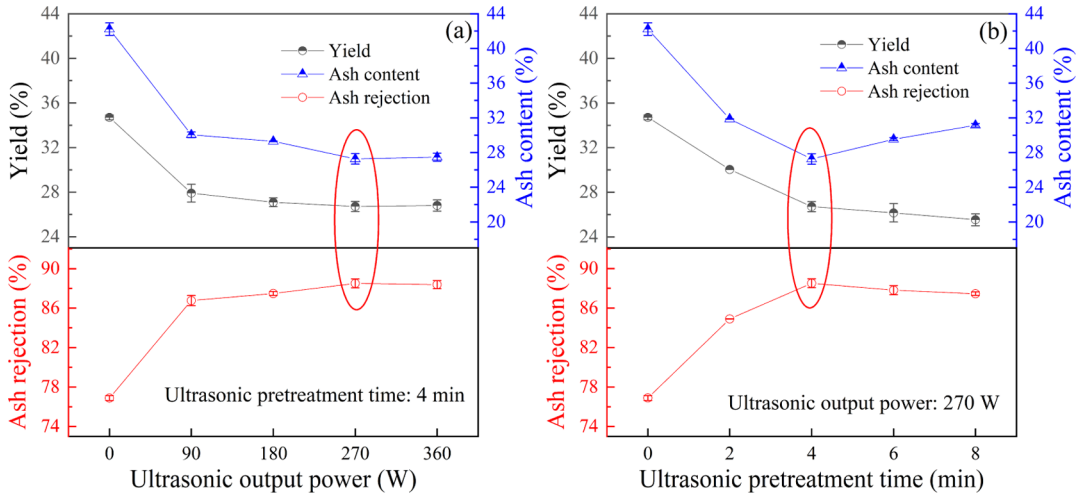

Figure 8. Yield, ash content, and AR of the concentrates as a function of the ultrasonic output power (a) and ultrasonic pretreatment time (b).

3.1.2. Morphology of the Different Particle Size Fractions. The apparent morphological features of the different particle size fractions are compared in Figure 6, with obviously visible effect of the ultrasonic treatment. Except for the 45−0 μm particle size fraction, all other fractions were observed to become "clean" after ultrasonic pretreatment, that is, the gray-white material (high ash fine particles) attached on the surface of larger particles was greatly reduced, thus, exposing more dark surfaces. The result was mainly due to the dispersion and cleaning effect of the ultrasonic radiations peeling off a large number of the high ash fine particles attached to the particle surface and subsequently exposing the intrinsic color of the large particles.[18] Moreover, compared with the conventional wet sieving, the +45 μm fractions were noted to be more "angular", probably due to the breakage of the particles caused by the ultrasonic crushing effect and subsequent generation of the new dissociation surface.

3.1.3. Yield and Ash Content in the Different Particle Size Fractions. As can be seen from Figure 7, with the increase in the ultrasonic output power and pretreatment time, the yield of the +250 μm fractions reduces, while that of the 45−0 μm fraction increases monotonically. However, the ash content of the +500 μm fraction increases on enhancing the ultrasonic output power, and the ash content of the fractions decreases except for the 250−125 μm fraction (the coarse particles with high ash content are dissociated by the ultrasonic treatment of high output power, for instance, 360 W), as shown in Figure 7a. This was probably owing to the reason that the increasing ultrasonic output power led to the fragmentation of a high extent of large particles with low ash content, or the diameter of the low ash content particles decreased, attributing to their inclusion in a smaller particle size fraction.[37] Besides, in Figure 7b, on extending the ultrasonic pretreatment time, the ash content of the +500 μm fraction first increases and subsequently decreases to some extent, whereas the ash content of the four 500−45 μm fractions shows an opposite trend. Therefore, the ultrasonic treatment for a long duration fragments the coarse particles with high ash content, resulting in their incorporation into smaller particle size fractions.

3.1.4. Residual Carbon Transfer Characteristics in Different Particle Size Fractions. The XFS exhibited obvious residual carbon enrichment characteristics in the particle size distributions in the natural state and after ultrasonic pretreatment. First, the low ash particles were mainly concentrated in the 500−250 μm fraction in the particle size distribution in the natural state. It was not cost-effective to separate this fraction by sieving, as it involved a two-stage wet sieving separation process, and the ash content and yield of the product were too high and low, respectively. Second, the ultrasonic pretreatment had a significant effect on the particle size distribution. The d_{80} value was noted to be significantly reduced, with the low ash particles more significantly enriched in the 500−250 μm and 250−125 μm fractions. Third, after ultrasonic pretreatment, the ash content of the +500 μm fraction increased, while that of the 125−75 μm fraction decreased. The ash content of the two fractions was basically identical and could be combined into the medium ash product; however, it was not appropriate considering the complicated separation process. Besides, although the yield of the 125−75 μm fraction was low, however, due to its high ash content, the overall content increased significantly on combining it in the concentrates. Therefore, the 125−75 μm fraction could be classified as the high ash particles and subsequently incorporated into the tailings. Fourth, although the yield of the +500 μm fraction was low, however, due to its high ash content, the overall content increased on combining it in the concentrates too. Moreover, the sieving separation of the 500 μm was straightforward and efficient; thus, the +500 μm fraction could be separately sieved as the middlings for further processing. In summary, the sample could be wet sieved into three products, including middlings containing the coarse particles with medium ash content (+500 μm), concentrates composed of the medium diameter particles with low ash content (500−125 μm) and tailings comprising of the fine particles with high ash content (125−0 μm). However, it was worth noting that there was an optimal set of conditions for ultrasonic pretreatment by quantifying the yield, quality, and AR of the concentrates.

3.2. Calculation of Concentrate Parameters.

3.2.1. Yield, Ash Content, and AR of Concentrates. As shown in Figure 8a, with the increase of the ultrasonic output power, the yield and ash content of the concentrates first decrease and then show a slight increase. At 270 W, AR was noted to reach its highest values, followed by a slight reduction. Similarly, in Figure 8b, on enhancing the ultrasonic pretreatment duration, the yield of the concentrates first decreases sharply for the ultrasonic output sustained at 270 W, followed

https://doi.org/10.1021/acsomega.2c05220
ACS Omega 2022, 7, 40306−40315

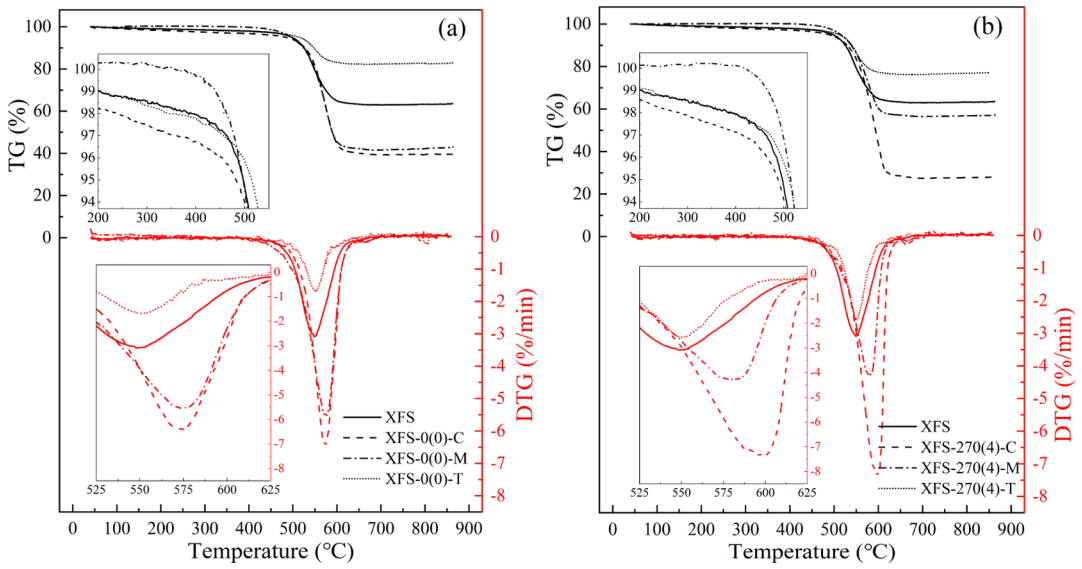

Figure 9. TG-DTG curves of the products of the conventional wet sieving (a) and ultrasonic wet sieving (b) separation processes.

by a gradual reduction. Furthermore, the ash content of the concentrates decreased obviously, whereas AR attained the highest value at 4 min. Therefore, the high ultrasonic output power and long pretreatment time did not result in a superior wet separation effect. At a low ultrasonic output power (0−90 W) or a short pretreatment time (0−2 min), the main effect of ultrasonication on the particle groups was cleaning and dispersion. At this stage, the high ash fine particles adhered on the surface of the low ash particles were transferred to the tailings due to the ultrasonic peeling and dispersion and thus sharply reducing the yield and ash content of the concentrates. Meanwhile, the low ash particles in the middlings were also stripped and dispersed by the ultrasonic action, subsequently transferring to the concentrates. This dynamic transfer made the AR of the concentrates to increase sharply. On increasing the ultrasonic output power or extending the ultrasonic pretreatment time, at a medium ultrasonic output power (90−270 W) or a medium pretreatment time (2−4 min), besides cleaning and dispersing, the main effect of the ultrasonic treatment on particle groups also included the fragmentation effect, which allowed a fraction of the low ash particles to transfer to the tailings. Meanwhile, the low ash particles in the middlings were stripped and dispersed by the ultrasonic action, followed by their transfer to the concentrates, which led to an enhanced ash content in the middlings. This comprehensive effect caused the AR of the concentrates to continue to increase slowly. However, at a higher ultrasonic output power (270−360 W) or a longer pretreatment time (4−8 min), the main effect of the ultrasonic treatment on particle groups also included the over-fragmented effect, resulting in a large extent of the low ash particles to be sieved to the tailings. Similarly, some high ash particles in the middlings were sieved to the concentrates and thus increasing the ash content and reducing the AR of the concentrates.

3.2.2. Determination of Optimum Sieving Separation Conditions. The pretreatment condition of ultrasonic output power of 270 W for 4 min was noted to be optimal considering the yield, ash content, and AR of the concentrates. Under this condition, the yield of the concentrates was 26.72%, indicating a reduction of 7.99% as compared to the conventional wet sieving. However, the observed reduction in yield was considered to be benign due to many reasons. On the one hand, the content of the fixed carbon for XFS was 31.78%, which indicated that a high yield of concentrates reflected a high ash content. On the other hand, the ultrasonic action reduced the adhesion of high-ash microbeads to low-ash particles, thus reducing ash entrainment in the concentrates.[38] Simultaneously, the ash content of the concentrates was 27.27%, which exhibited a reduction of 14.96% as compared to the conventional wet sieving. Besides, the AR of concentrates was 88.51%, which was increased by 11.63% as compared to the conventional wet sieving. Hence, the quality of the concentrates and residual carbon enrichment efficiency were significantly improved by the wet sieving separation with ultrasonic pretreatment.

3.3. Combustion Characteristics of the Samples.

3.3.1. hermogravimetric Analysis. Figure 9 illustrates the TG-DTG curves of the products after the conventional and ultrasonic wet sieving separation processes. The XFS-0(0)-T exhibited the lowest weight loss, indicating the low residual carbon content of the tailings in the conventional sieving. Although the extent of weight loss in XFS-0(0)-C was noted to be higher than that of XFS-0(0)-M, however, the overall weight loss in the samples was very low. The result indicated that the concentrates and middlings in the conventional sieving had not been separated effectively. However, in the case of the products of the ultrasonic pretreatment wet sieving separation, as shown in Figure 9b, XFS-270(4)-T shows the lowest weight loss, as some low ash particles are transferred to the tailings. Simultaneously, the weight loss percentage in XFS-270(4)-M was observed to be significantly lower than that of XFS-0(0)-M, as the residual carbon in the middlings transferred to the concentrates after ultrasonic pretreatment. Besides, XFS-270(4)-C had the highest weight loss percentage and carbon content. It should be noted that both XFS-0(0)-M and XFS-270(4)-M exhibited an obvious negative weight loss (weight gain) process before 400 °C as the chemical oxygen absorption of the sample exceeded the low-temperature oxidation of the samples, which might be related to the unique structure and composition of the coarse particles.

3.3.2. Characteristic Combustion Parameters. The characteristic combustion parameters of the tested samples are

https://doi.org/10.1021/acsomega.2c05220
ACS Omega 2022, 7, 40306−40315

Table 2. Characteristic Combustion Parameters From the TG-DTG Curves

samples	T_i/°C	T_{peak}/°C	T_h/°C	dW_{max}/%·min^{-1}	dW_{mean}/%·min^{-1}	C/%·min^{-1}·°C^{-2}	S/%^{2}·min^{-2}·°C^{-3}
XFS	513.68	548.63	581.03	3.09	0.29	1.17×10^{-5}	5.78×10^{-9}
XFS-0(0)-M	534.12	572.36	597.04	5.54	0.52	1.94×10^{-5}	1.69×10^{-8}
XFS-0(0)-C	536.04	574.79	597.30	6.40	0.53	2.23×10^{-5}	1.97×10^{-8}
XFS-0(0)-T	506.73	550.82	578.50	1.68	0.16	6.56×10^{-6}	1.78×10^{-9}
XFS-270(4)-M	532.25	581.25	602.70	4.29	0.38	1.51×10^{-5}	9.59×10^{-9}
XFS-270(4)-C	544.25	596.90	615.57	7.33	0.79	2.48×10^{-5}	3.17×10^{-8}
XFS-270(4)-T	511.91	550.40	579.19	2.57	0.18	9.82×10^{-6}	3.00×10^{-9}

compared in Table 2. It was noted that the ignition and burnout point temperatures for the XFS, XFS-0(0)-C, and XFS-270(4)-C were 513.68 and 581.03, 536.04 and 597.30, and 544.25 and 615.57 °C, respectively, which increased with the increase in the carbon content (as shown in Table 1). Meanwhile, the dW_{max} and dW_{mean} for the XFS-270(4)-C at 7.33 and 0.79, respectively, were higher than those of XFS and XFS-0(0)-C. This result might be related to the generation of the fine cinders during coal gasification as well as the transfer rule of the residual carbon and residue in the gasifier. Wu et al.[39] reported that the residual carbon in the entrained-flow gasification coal fine slag mainly included three parts, viz. "partial volatile matter of raw coal pyrolysis", "partly gasified carbon", and "unreacted pyrolytic carbon". The partial volatile matter of the raw coal pyrolysis mainly existed below 75 μm, which contained a small residual carbon content and was not swiftly gasified in the gasifier due to being wrapped by the inorganic molten ash. Thus, it resulted in the volatile substances being retained in the particles, forming residual carbon. The partly gasified carbon mainly existed in the medium particle size fractions, and the content was much higher mainly due to the short residence time in the gasifier and incomplete gasification. The unreacted pyrolytic carbon, the unburnt char captured by the flowing slag, was wrapped in the inorganic ash which cannot be directly combined with the gasification agent, and its particle size was generally large. Moreover, the relevant studies have shown that the reactivity of the three residual carbons followed the following sequence: partial volatile matter of raw coal pyrolysis > unreacted pyrolytic carbon > partly gasified carbon. Therefore, although XFS-0(0)-T had the lowest carbon content, it had the highest V_{daf} and the lowest ignition point and burnout point temperatures. The XFS-270(4)-T contained a higher extent of the low activity carbon content than XFS-0(0)-T, which led to a slight enhancement in the ignition point and burnout point temperatures. In addition, it could be inferred that, after ultrasonic pretreatment, a part of the low activity residual carbon in XFS-0(0)-M was transferred to the concentrates, which reduced the carbon content, ignition point, and burnout point temperature of the middlings. In other words, XFS-270(4)-C had a high extent of the enriched low activity residual carbon, leading to the enhanced ignition point and burnout point temperatures and reduced activity of the concentrates.

Despite the lowest reactivity and V_{daf}, XFS-270(4)-C exhibits a low ash content (27.27%), a high carbon content (nearly 70%), the highest maximum weight loss rate (7.33%·min^{-1}), and the highest C, S, and HHV values, as shown in Table 1. These results indicated that the concentrates in the ultrasonic pretreatment wet sieving separation displayed the optimal combustion performance. Therefore, ultrasonic pretreatment had a positive effect on the residual carbon enrichment in the concentrates.

4. CONCLUSIONS

In this work, the residual carbon in the entrained-flow gasification coal fine slag was enriched via employing a combination of ultrasonic pretreatment and wet sieving process, along with achieving the reduced ash content and improved combustion performance of the concentrates. The findings from this work provided new solutions for the separation and utilization of the coal gasification fine slag. The following conclusions could be drawn:

1 After the ultrasonic pretreatment, the residual carbon enrichment pattern in the particle size distribution for coal gasification fine slags was mainly enriched toward the 500−250 μm and 250−125 μm particle size classes, as compared to conventional wet screening.

2 Considering the yield, ash content, and AR of the concentrates, the optimal ultrasonic pretreatment conditions for wet sieving process were 270 W for 4 min. Under these conditions, the yield and ash content of the concentrate were 26.72 and 27.27% respectively, with an AR rate of 88.51%.

3 TG-DTG confirmed that the concentrates from the ultrasonic pretreatment (270 W for 4 min) wet sieving separation could reduce the chemical reactivity of the experimental samples. Meanwhile, they also had the lower ash content (27.27%) and the higher carbon content (nearly 70%), maximum weight loss rate (7.33%·min^{-1}), and HHV.

4 The combustion characteristics analysis showed that the residual carbon was enriched in the concentrate and its combustion performance was significantly improved. The composite combustion characteristic index of 3.17×10^{-8} for the wet screening concentrate after ultrasonic pretreatment was significantly higher than the values of 5.78×10^{-9} and 1.97×10^{-8} for the raw and conventional screening concentrates, respectively.

Therefore, the combination of ultrasonic pretreatment and wet sieving process is an effective way to achieve the goal of "harmlessness, recycling, and utilization" for the coal gasification slags.

AUTHOR INFORMATION

Corresponding Author

Dinghua Liu − *Suzhou Sinoma Design and Research Institute of Non-Metallic Minerals Industry Co., Ltd., Suzhou 215151, China; National Engineering Research Center for Further Processing of Non-Metallic Minerals, Suzhou 215151, China*; Email: 15650700916@163.com

https://doi.org/10.1021/acsomega.2c05220
ACS Omega 2022, 7, 40306−40315

Authors

Meijie Sun − *School of Chemical and Environmental Engineering, China University of Mining & Technology (Beijing), Beijing 100083, China;* orcid.org/0000-0003-4808-2167

Suqian Gu − *School of Chemical and Environmental Engineering, China University of Mining & Technology (Beijing), Beijing 100083, China*

Zhiqiang Xu − *School of Chemical and Environmental Engineering, China University of Mining & Technology (Beijing), Beijing 100083, China*

Weidong Wang − *School of Chemical and Environmental Engineering, China University of Mining & Technology (Beijing), Beijing 100083, China*

Yanan Tu − *School of Chemical and Environmental Engineering, China University of Mining & Technology (Beijing), Beijing 100083, China*

Lufan Wang − *School of Chemical and Environmental Engineering, China University of Mining & Technology (Beijing), Beijing 100083, China*

Haiyan Liu − *School of Chemical and Environmental Engineering, China University of Mining & Technology (Beijing), Beijing 100083, China*

Sijia Lu − *School of Chemical and Environmental Engineering, China University of Mining & Technology (Beijing), Beijing 100083, China*

Complete contact information is available at: https://pubs.acs.org/10.1021/acsomega.2c05220

Notes

The authors declare no competing financial interest.

■ ACKNOWLEDGMENTS

The authors gratefully acknowledge the financial support provided by the China National Nature Science Foundation (no.51974325) and the Fundamental Research Funds for the Central Universities (no.2022XJHH05).

■ REFERENCES

(1) Liu, S.; Zhao, H.; Liu, X.; Li, Y.; Zhao, G.; Wang, Y.; Zeng, M. Effect of a combined process on pyrolysis behavior of huolinhe lignite and its kinetic analysis. *Fuel* **2020**, *279*, 118485.

(2) Liu, S.; Zhou, Q.; Li, G.; Feng, L.; Zhang, Q.; Weng, X.; Zhang, J.; Ma, Z. Removal of O-containing functional groups during hydrothermal treatment dewatering: A combined experimental and theoretical theory study. *Fuel* **2022**, *326*, 124971.

(3) Liu, S.; Qi, C.; Jiang, Z.; Zhang, Y.; Niu, M.; Li, Y.; Dai, S.; Finkelman, R. B. Mineralogy and geochemistry of ash and slag from coal gasification in China: a review. *Int. Geol. Rev.* **2017**, *60*, 717−735.

(4) Xu, S.; Zhou, Z.; Gao, X.; Yu, G.; Gong, X. The gasification reactivity of unburned carbon present in gasification slag from entrained-flow gasifier. *Fuel Process. Technol.* **2009**, *90*, 1062−1070.

(5) Guo, X.; Tang, Y.; Wang, Y.; Eble, C. F.; Finkelman, R. B.; Li, P. Evaluation of carbon forms and elements composition in coal gasification solid residues and their potential utilization from a view of coal geology. *Waste Manag* **2020**, *114*, 287−298.

(6) Guo, F.; Miao, Z.; Guo, Z.; Li, J.; Zhang, Y.; Wu, J. Properties of flotation residual carbon from gasification fine slag. *Fuel* **2020**, *267*, 117043.

(7) Zhao, X.; Zeng, C.; Mao, Y.; Li, W.; Peng, Y.; Wang, T.; Eiteneer, B.; Zamansky, V.; Fletcher, T. The Surface Characteristics and Reactivity of Residual Carbon in Coal Gasification Slag. *Energy Fuels* **2010**, *24*, 91−94.

(8) Dai, G.; Zheng, S.; Wang, X.; Bai, Y.; Dong, Y.; Du, J.; Sun, X.; Tan, H. Combustibility analysis of high-carbon fine slags from an entrained flow gasifier. *J. Environ. Manage.* **2020**, *271*, 111009.

(9) Yang, Y.; Chu, M.; Shi, X.; Lyu, F.; Sun, X.; Jia, C. Grading Characteristics of Texaco Gasification Fine Slag: Quality Distinction and Selective Distribution of Trace Elements. *ACS Omega* **2020**, *5*, 26883−26893.

(10) Guo, F.; Guo, Y.; Guo, Z.; Miao, Z.; Zhao, X.; Zhang, Y.; Li, J.; Wu, J. Recycling Residual Carbon from Gasification Fine Slag and Its Application for Preparing Slurry Fuels. *ACS Sustainable Chem. Eng.* **2020**, *8*, 8830−8839.

(11) Guo, F.; Zhao, X.; Guo, Y.; Zhang, Y.; Wu, J. Fractal analysis and pore structure of gasification fine slag and its flotation residual carbon. *Colloids Surf. A Physicochem. Eng. Aspects* **2020**, *585*, 124148.

(12) Zhang, R.; Guo, F.; Xia, Y.; Tan, J.; Xing, Y.; Gui, X. Recovering unburned carbon from gasification fly ash using saline water. *Waste Manag* **2019**, *98*, 29−36.

(13) Liu, S.; Wei, J.; Chen, X.; Ai, W.; Wei, C. Low-Cost Route for Preparing Carbon−Silica Composite Mesoporous Material from Coal Gasification Slag: Synthesis, Characterization and Application in Purifying Dye Wastewater. *Arabian J. Sci. Eng.* **2020**, *45*, 4647−4657.

(14) Pan, C.; Liang, Q.; Guo, X.; Dai, Z.; Liu, H.; Gong, X. Characteristics of Different Sized Slag Particles from Entrained-Flow Coal Gasification. *Energy Fuels* **2016**, *30*, 1487−1495.

(15) Wu, T.; Gong, M.; Lester, E.; Wang, F.; Zhou, Z.; Yu, Z. Characterisation of residual carbon from entrained-bed coal water slurry gasifiers. *Fuel* **2007**, *86*, 972−982.

(16) Liu, D.; Wang, W.; Tu, Y.; Ren, G.; Yan, S.; Liu, H.; He, H. Flotation specificity of coal gasification fine slag based on release analysis. *J. Clean. Prod.* **2022**, *363*, 132426.

(17) Sousa, R.; Futuro, A.; Fiúza, A.; Leite, M. M. Pre-concentration at crushing sizes for low-grade ores processing − Ore macro texture characterization and liberation assessment. *Miner. Eng.* **2020**, *147*, 106156.

(18) Wang, W.; Liu, D.; Tu, Y.; Jin, L.; Wang, H. Enrichment of residual carbon in entrained-flow gasification coal fine slag by ultrasonic flotation. *Fuel* **2020**, *278*, 118195.

(19) Kursun, H. A Study on the Utilization of Ultrasonic Pretreatment in Zinc Flotation. *Sep. Sci. Technol.* **2014**, *49*, 2975−2980.

(20) Peng, Y.; Mao, Y.; Xia, W.; Li, Y. Ultrasonic flotation cleaning of high-ash lignite and its mechanism. *Fuel* **2018**, *220*, 558−566.

(21) Kang, W.; Xun, H.; Hu, J. Study of the effect of ultrasonic treatment on the surface composition and the flotation performance of high-sulfur coal. *Fuel Process. Technol.* **2008**, *89*, 1337−1344.

(22) Mao, Y.; Xia, W.; Peng, Y.; Xie, G. Ultrasonic-assisted flotation of fine coal: A review. *Fuel Process. Technol.* **2019**, *195*, 106150.

(23) Zhang, T.; He, Y.; Wang, F.; Ge, L.; Zhu, X.; Li, H. Chemical and process mineralogical characterizations of spent lithium-ion batteries: an approach by multi-analytical techniques. *Waste Manag* **2014**, *34*, 1051−1058.

(24) Acar, I.; Atalay, M. U. Recovery potentials of cenospheres from bituminous coal fly ashes. *Fuel* **2016**, *180*, 97−105.

(25) De Boom, A.; Degrez, M. Combining sieving and washing, a way to treat MSWI boiler fly ash. *Waste Manag* **2015**, *39*, 179−188.

(26) Sun, M.; Zheng, J.; Liu, X. Effect of Hydrothermal Dehydration on the Slurry Ability of Lignite. *ACS Omega* **2021**, *6*, 12027−12035.

(27) Gu, S.; Xu, Z.; Ren, Y.; Tu, Y.; Sun, M.; Liu, X. An approach for upgrading lignite to improve slurryability: Blending with direct coal liquefaction residue under microwave-assisted pyrolysis. *Energy* **2021**, *222*, 120012.

(28) Majumder, A.; Jain, R.; Banerjee, P.; Barnwal, J. Development of a new proximate analysis based correlation to predict calorific value of coal. *Fuel* **2008**, *87*, 3077−3081.

(29) Oruç, F.; Özgen, S.; Sabah, E. An enhanced-gravity method to recover ultra-fine coal from tailings: Falcon concentrator. *Fuel* **2010**, *89*, 2433−2437.

(30) Sahinoglu, E.; Uslu, T. Increasing coal quality by oil agglomeration after ultrasonic treatment. *Fuel Process. Technol.* **2013**, *116*, 332−338.
(31) Liu, S.; Zhao, H.; Liu, X.; Li, Y.; Zhao, G.; Wang, Y.; Zeng, M. Effect of hydrothermal upgrading on the pyrolysis and gasification characteristics of baiyinhua lignite and a mechanistic analysis. *Fuel* **2020**, *276*, 118081.
(32) Gu, S.; Xu, Z.; Ren, Y.; Zhang, Y.; Tu, Y. Energy utilization of direct coal liquefaction residue via co-slurry with lignite: Slurryability, combustion characteristics, and their typical pollutant emissions. *Fuel* **2022**, *326*, 125037.
(33) Gu, S.; Xu, Z.; Ren, Y.; Tu, Y.; Lu, D.; Wang, H. Microwave co-pyrolysis of lignite with direct coal liquefaction residue: Synergistic effects and product combustion characteristics. *J. Clean. Prod.* **2021**, *325*, 129293.
(34) Kuan, Y.-H.; Wu, F.-H.; Chen, G.-B.; Lin, H.-T.; Lin, T.-H. Study of the combustion characteristics of sewage sludge pyrolysis oil, heavy fuel oil, and their blends. *Energy* **2020**, *201*, 117559.
(35) Wang, X.; Si, J.; Tan, H.; Niu, Y.; Xu, C.; Xu, T. Kinetics investigation on the combustion of waste capsicum stalks in Western China using thermogravimetric analysis. *J. Therm. Anal. Calorim.* **2011**, *109*, 403−412.
(36) Mao, Y.; Bu, X.; Peng, Y.; Tian, F.; Xie, G. Effects of simultaneous ultrasonic treatment on the separation selectivity and flotation kinetics of high-ash lignite. *Fuel* **2020**, *259*, 116270.
(37) Xue, Z.; Dong, L.; Fan, X.; Ren, Z.; Liu, X.; Fan, P.; Fan, M.; Bao, W.; Wang, J. Physical and Chemical Properties of Coal Gasification Fine Slag and Its Carbon Products by Hydrophobic-Hydrophilic Separation. *ACS Omega* **2022**, *7*, 16484−16493.
(38) Niu, M.; Fu, Y.; Liu, S. Mineralogical Characterization of Gasification Ash with Different Particle Sizes from Lurgi Gasifier in the Coal-to-Synthetic Natural Gas Plant. *ACS Omega* **2022**, *7*, 8526−8535.
(39) Wu, S.; Huang, S.; Ji, L.; Wu, Y.; Gao, J. Structure characteristics and gasification activity of residual carbon from entrained-flow coal gasification slag. *Fuel* **2014**, *122*, 67−75.

https://doi.org/10.1021/acsomega.2c05220
ACS Omega 2022, 7, 40306−40315